COMMUNICATIONS IN COMPUTATIONAL PHYSICS
Vol. **4**, No. 3, pp. 575-591

Commun. Comput. Phys.
September 2008

Electromagnetic High Frequency Gyrokinetic Particle-in-Cell Simulation

R. A. Kolesnikov*, W. W. Lee and H. Qin

Plasma Physics Laboratory, Princeton University, P.O. Box 451, Princeton, New Jersey 08543, USA.

Received 29 October 2007; Accepted (in revised version) 6 March 2008

Available online 14 April 2008

Abstract. Using the gyrocenter-gauge kinetic theory, an electromagnetic version of the high frequency gyrokinetic numerical algorithm for particle-in-cell simulation has been developed. The new algorithm, being an alternative to a direct Lorentz-force simulation, offers an efficient way to simulate the dynamics of plasma heating and current drive with radio frequency waves. Gyrokinetic formalism enables separation of gyrocenter and gyrophase motions of a particle in a strong magnetic field. From this point of view, a particle may be viewed as a combination of a slow gyrocenter and a quickly changing Kruskal ring. In this approach, the nonlinear dynamics of high frequency waves is described by the evolution of Kruskal rings based on first principles physics. The efficiency of the algorithm is due to the fact that the simulation particles are advanced along the slow gyrocenter orbits, while the Kruskal rings capture fast gyrophase physics. Moreover, the gyrokinetic formalism allows separation of the cold response from kinetic effects in the current, which allows one to use much smaller number of particles than what is required by a direct Lorentz-force simulation. Also, the new algorithm offers the possibility to have particle refinement together with mesh refinement, when necessary. To illustrate the new algorithm, a simulation of the electromagnetic low-hybrid wave propagating in inhomogeneous magnetic field is presented.

PACS: 52.30.Gz, 52.25.Xz, 52.25.Dg
Key words: Gyrokinetics, magnetized plasmas, plasma kinetic equations.

1 Introduction

The gyrokinetic theory [1–3] is normally known as a tool for description of the low frequency dynamics of plasmas in a strong magnetic field. Changing variables to a gyrocenter coordinate system in the original Vlasov and Maxwell's equations, the gyrokinetic

*Corresponding author. *Email addresses:* rkolesni@pppl.gov (R. A. Kolesnikov), wwlee@pppl.gov (W. W. Lee), hongqin@pppl.gov (H. Qin)

formalism yields a system of gyrophase-independent equations, which describe slow (alternatively, low frequency with $\omega \ll \Omega$, where Ω is the cyclotron frequency) phenomena in plasmas. However, the physics associated with the omitted fast gyrophase part may be important. Particularly, in fusion plasmas, radio frequency (rf) waves in both ion and electron cyclotron frequency ranges are used for plasma heating and current drive. In this paper we present a computational algorithm, which is an alternative to direct Lorentz-force simulation and which allows one to numerically study an arbitrary frequency dynamics of plasmas within the gyrokinetic framework. This paper addresses electromagnetic version of the algorithm developed in the previous work by Kolesnikov *et al.* [4,5].

The high frequency gyrokinetic approach we discuss in this paper is based on the gyrocenter-gauge kinetic theory, developed by Qin *et al.* [6–8] in the limit of particle gyroradius much smaller than the scale length of the ambient magnetic field, $\rho/L_B \ll 1$ (in the case of strongly magnetized plasmas). The gyrokinetic formalism transforms the Vlasov-Maxwell system in 6D particle coordinate system $\boldsymbol{z}=(\boldsymbol{x},\boldsymbol{v})$ to a new 6D gyrocenter system $\boldsymbol{Z}=(\boldsymbol{X},U,\mu,\xi)$. Here, $\boldsymbol{X}$ and U are the location and parallel velocity of the particle gyrocenter, μ is the magnetic moment and ξ is the gyrophase angle. While $F(\boldsymbol{x},\boldsymbol{v},t)$ is the distribution function in the old particle coordinates, $F(\boldsymbol{Z},t)$ is the distribution function in the new coordinates, where the parallel (gyrocenter) and the perpendicular (gyrophase) dynamics are decoupled, such that

$$F(\boldsymbol{Z},t)=\langle F(\boldsymbol{Z},t)\rangle. \tag{1.1}$$

Here, the notation for a gyrophase-averaged quantity is introduced by

$$\langle a\rangle \doteq (2\pi)^{-1}\int a d\xi.$$

All the fast gyrophase dynamics is completely captured by, so called, gauge function $S(\boldsymbol{Z},t)$. Similar approach was used by Lee *et al.* [9] and Park *et al.* [10] for treatment of arbitrary frequency dynamics.

An algorithm based on gyrokinetics may prove useful if we need to add an arbitrary frequency dynamics, like rf waves, into existing sophisticated gyrokinetic particle codes [11] developed to study low frequency turbulence phenomena in general geometry. Also, the new algorithm may be much more computationally effective than the direct Lorentz-force integration. There are several reasons for this. First, the motion of gyrocenters is slow; larger time step may be used for simulation of their dynamics, thus saving some computing time. Second, cold response may be separated from the kinetic effects in the expression for the current, which will allow to reduce the total number of particles required in the simulation. Third, the algorithm allows adaptive particle refinement together with mesh refinement, a feature important for the systems with different spatial scales. This paper will address these issues in more detail.

We believe that our new approach may be especially useful for computational study of the dynamics of propagation, conversion and absorption of radio frequency waves

[12–14] in tokamak plasmas. Similar to a Lorentz-force simulation, the high frequency gyrokinetic algorithm allows completely self-consistent simulation. Also, it can describe both linear and nonlinear heating dynamics based on first principle physics without extra assumptions about quasilinear nature of heating mechanism.

This paper is organized as follows. In Section 2 we briefly review the gyrocenter gauge kinetic theory, which underlies our electromagnetic high frequency gyrokinetic system of equations. The 6D algorithm based on this system is described in Section 3 with application to propagation of the low-hybrid wave in inhomogeneous magnetic field in 3D slab. In Section 4 we address the possibility to have particle refinement and mesh refinement coexisting dynamically in the system with different spatial scales. The conclusions and future work are presented in Section 5.

2 Electromagnetic high frequency gyrokinetic formalism

The idea of the gyrokinetics is to identify a certain sequence of transformations from the original particle coordinates $\boldsymbol{z}$ to a new gyrocenter coordinate system $\boldsymbol{Z}$

$$\boldsymbol{Z}=\mathsf{T}_{GY}\mathsf{T}_{GC}\boldsymbol{z}. \tag{2.1}$$

Here T_{GC} and T_{GY} stand for guiding center and gyrocenter transformations accordingly. One needs to make sure that the original Vlasov equation for the distribution function $F(\boldsymbol{x},\boldsymbol{v},t)$ in particle coordinates

$$\Big(\frac{\partial}{\partial t}+\dot{\boldsymbol{x}}\cdot\frac{\partial}{\partial \boldsymbol{x}}+\dot{\boldsymbol{v}}\frac{\partial}{\partial \boldsymbol{v}}\Big)F=0 \tag{2.2}$$

transforms to an equation for the slow gyrophase-independent part of the distribution function $F(\boldsymbol{Z},t)=\langle F(\boldsymbol{Z},t)\rangle$. It describes the evolution of the gyrocenter (parallel) dynamics according to

$$\frac{dF}{dt}\doteq\Big(\frac{\partial}{\partial t}+\dot{\boldsymbol{X}}\cdot\frac{\partial}{\partial \boldsymbol{X}}+\dot{U}\frac{\partial}{\partial U}\Big)F=0. \tag{2.3}$$

The relation between different distribution functions is given by

$$F(\boldsymbol{x},\boldsymbol{v},t)=\mathsf{T}^{*}_{GY}\mathsf{T}^{*}_{GC}F(\boldsymbol{Z},t), \tag{2.4}$$

where T^{*}_{GC} and T^{*}_{GY} are pull-back transformations, which transform the perturbed distribution functions between particles and guiding center, and guiding center and gyrocenter coordinates accordingly.

The near identity transformation

$$\mathsf{T}^{*}_{GY}=1+\delta\mathsf{T} \tag{2.5}$$

depends on a special gauge [6] function $S(\boldsymbol{Z},t)$, which contains fast gyrophase (perpendicular) part of the dynamics. For an electromagnetic system

$$\begin{aligned}\delta \mathsf{T} F(\boldsymbol{Z},t) \doteq & \frac{q}{mc}\Big(\frac{q}{c}\boldsymbol{A}\cdot\frac{\partial \boldsymbol{\rho}_0}{\partial \xi}+\frac{\partial S}{\partial \xi}\Big)\frac{\partial \ln F}{\partial \mu}\\ &+\frac{q}{mc}\widehat{\boldsymbol{b}}\cdot\Big(\boldsymbol{A}+\frac{c}{q}\frac{\partial S}{\partial \boldsymbol{X}}\Big)\frac{\partial \ln F}{\partial U}\\ &-\frac{\widehat{\boldsymbol{b}}}{B_0}\times\Big(\boldsymbol{A}+\frac{c}{q}\frac{\partial S}{\partial \boldsymbol{X}}\Big)\cdot\frac{\partial \ln F}{\partial \boldsymbol{X}}.\end{aligned} \tag{2.6}$$

Here the following partition of the electromagnetic field is used

$$\boldsymbol{B}=\boldsymbol{B}_0+\boldsymbol{B}_1,\quad \boldsymbol{E}=\boldsymbol{E}_1,\quad \boldsymbol{B}_1=\nabla\times\boldsymbol{A}, \tag{2.7}$$

where $\boldsymbol{B}_0$ is the equilibrium background magnetic field, $\boldsymbol{B}_1$ and $\boldsymbol{E}_1$ are the perturbed fields and $\boldsymbol{A}$ is a vector potential.

The gauge function $S(\boldsymbol{Z},t)$ evolves according to

$$\begin{aligned}\dot{S} \doteq & \Big(\frac{d}{dt}+\Omega_0\frac{\partial}{\partial \xi}\Big)S\\ = & q\widetilde{\Phi}(\boldsymbol{X}+\boldsymbol{\rho},t)-\frac{e}{c}\widetilde{\boldsymbol{V}\cdot\boldsymbol{A}}(\boldsymbol{X}+\boldsymbol{\rho},t),\end{aligned} \tag{2.8}$$

where $\boldsymbol{V}=\boldsymbol{v}_\perp+U\widehat{\boldsymbol{b}}$ and $\widetilde{a}\doteq a-\langle a\rangle$. The cyclotron frequency is calculated at gyrocenter location

$$\Omega_0=\frac{e}{mc}B_0(\boldsymbol{X}). \tag{2.9}$$

New coordinates $\boldsymbol{Z}$ make sure that the gyrophase dependence is completely contained in the Eq. (2.8).

An appropriate conserved adiabatic invariant μ is obtained by expanding up to the first order term in the smallness parameter $\rho/L_B\ll 1$, and is given by

$$\mu=\frac{mv_\perp^2}{2B_0(\boldsymbol{X})}+\frac{q}{mc}\Big(\frac{q}{c}\boldsymbol{A}(\boldsymbol{X}+\boldsymbol{\rho}_0,t)\cdot\frac{\partial \boldsymbol{\rho}_0}{\partial \xi}+\frac{\partial S}{\partial \xi}\Big). \tag{2.10}$$

The quantity μ is an approximation to the true magnetic moment, which contains all orders in expansion in the smallness parameter. Eqs. (2.8) and (2.10) describe nonlinear perpendicular dynamics of a particle around the cyclotron resonance. Note that exact resonances are also allowed as long as they happen locally in space and during short intervals of time. This is necessary to make sure that the increment in $v_\perp$ in Eq. (2.10) is small (compared to $v_\perp$) during each of these wave-particle interactions near resonances, which is the case in tokamak experiments.

Self-consistency is obtained by solving Ampere's and Faraday's laws

$$\frac{\partial}{\partial t}\boldsymbol{E}_1(\boldsymbol{x},t)=c\nabla\times\boldsymbol{B}_1(\boldsymbol{x},t)-4\pi\boldsymbol{J}(\boldsymbol{x},t), \tag{2.11}$$

$$\frac{\partial}{\partial t}\boldsymbol{B}_1(\boldsymbol{x},t)=-c\nabla\times\boldsymbol{E}_1(\boldsymbol{x},t). \tag{2.12}$$

The current on the right hand side is given by the following expression

$$\begin{aligned}\boldsymbol{J}(\boldsymbol{x},t)&=\sum_s q_s\int \boldsymbol{v}F_s(\boldsymbol{x},\boldsymbol{v},t)d\boldsymbol{v}\\ &=\sum_s q_s\int(\boldsymbol{v}_\perp+U\widehat{\boldsymbol{b}})[(1+\delta\mathsf{T})F_s(\boldsymbol{Z},t)]\delta(\boldsymbol{X}-\boldsymbol{x}+\boldsymbol{\rho})d\boldsymbol{Z},\end{aligned} \tag{2.13}$$

where s stands for species. In the gyrocenter coordinates a near-identity transformation Eq. (2.5) divides the particle current (2.13) into two parts. The first part is due to the gyrocenter distribution function $F(\boldsymbol{Z},t)$. The second part is the contribution due to the gyrophase dependent part of the distribution function, which describes polarization effects due to gyromotion.

3 Numerical algorithm

The low frequency electrostatic gyrokinetics only solves Eq. (2.3) along with an appropriate gyrokinetic Poisson equation [2]. Instead of individual particle's trajectories, the low frequency gyrokinetics sees motion of gyrocenters with rigid uniformly charged rings attached to them (Fig. 1(a)). The purpose of these rings is to take FLR effects into account by appropriate averaging technique via a finite number of points on each ring [15].

For the arbitrary electromagnetic frequency case, Eqs. (2.3) and (2.8) for the gyrocenter and gyrophase dynamics need to be solved together with the Maxwell's Eqs. (2.11)-(2.12) and the conservation of the magnetic moment (2.10). The gyrocenter dynamics described by the Eq. (2.3) is easily simulated by a *gyrocenter pusher* [15], which advances each particle's gyrocenter location $\boldsymbol{X}$ and parallel velocity U. Also, if δf-simulation [16] is used, then each particle will also have a gyrocenter weight $w_j=\delta f/F|_j$ associated with it. Here $F=F_0+\delta f$, with F_0 being the background distribution function.

The gyrophase dependent part of the dynamics described by the equation for the generating function (2.8) may be simulated by a *gyrophase pusher*, which solves the functions $g_{\mathsf{T}}(\boldsymbol{Z},t)$ and $g_{\xi}(\boldsymbol{Z},t)$, where

$$g_{\mathsf{T}}\doteq\widehat{Q}_{\mathsf{T}}S,\quad g_{\xi}\doteq\widehat{Q}_{\xi}S, \tag{3.1}$$

and the operators are given by the following expressions

$$\widehat{Q}_{\mathsf{T}}\doteq\frac{q}{mc}\frac{\partial\ln F_0}{\partial\mu}\frac{\partial}{\partial\xi}+\frac{1}{m}\widehat{\boldsymbol{b}}\cdot\frac{\partial\ln F_0}{\partial U}\frac{\partial}{\partial\boldsymbol{X}}-\frac{c}{q}\frac{\partial\ln F_0}{\partial\boldsymbol{X}}\cdot\Big(\frac{\widehat{\boldsymbol{b}}}{B_0}\times\frac{\partial}{\partial\boldsymbol{X}}\Big), \tag{3.2}$$

$$\widehat{Q}_{\xi}\doteq\frac{q}{mc}\frac{\partial}{\partial\xi}. \tag{3.3}$$

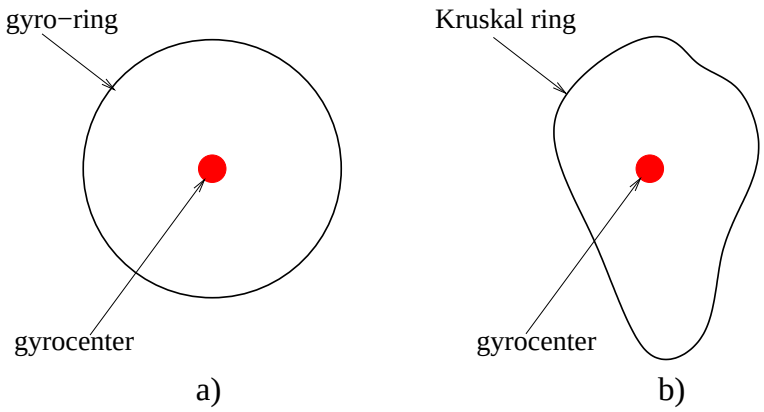

Figure 1: A particle from the point of view of low frequency (a) and high frequency (b) gyrokinetics.

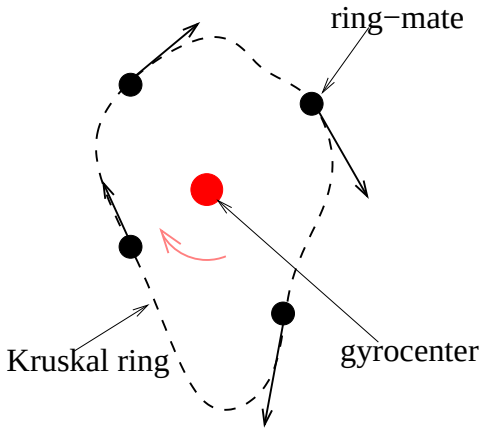

Figure 2: A Kruskal ring is approximated by a finite number of ring-mates.

In the arbitrary frequency regime, the motion of particles from the gyrokinetic point of view is more complicated than in the low frequency regime. Particularly, instead of individual particle's trajectories, the arbitrary frequency gyrokinetics sees motion of gyrocenters together with *Kruskal rings* [17] (Fig. 1(b)) attached to them. As before, the motion of a gyrocenter j is according to Eq. (2.3). In real simulation, only a finite number of points (*ring-mates* [18]) p on each Kruskal ring are followed (Fig. 2). For a particular gyrocenter j, we use index l to enumerate simulation ring-mates (which have the same $\boldsymbol{X}_j$ and U_j, but different ξ_l's) on its Kruskal ring. Each of these ring-mates has a *gyrophase weight* $g_{\mathsf{T}}(\boldsymbol{Z}_{jl},t)$ attached to it, which evolves according to

$$\dot{g}_{\mathsf{T}}(\boldsymbol{Z}_{jl},t)=\widehat{Q}_{\mathsf{T}jl}\left(q\widetilde{\Phi}_{jl}-\frac{e}{c}\widetilde{\boldsymbol{V}_{jl}\cdot\boldsymbol{A}_{jl}}\right). \tag{3.4}$$

Here a new notation is introduced by

$$a_{jl}\doteq a(\boldsymbol{X}_j+\boldsymbol{\rho}_j(\xi_l)). \tag{3.5}$$

Then the dynamics of ring-mate l is determined by the rotation with the cyclotron frequency $\dot{\xi}_l = \Omega_0$, together with conservation of the magnetic moment $\mu_j(\xi_l) = \text{const}$, which takes the following form

$$\mu_j(\xi_l) = \frac{v_{\perp j}^2(\xi_l,t)}{2B_0(\boldsymbol{X}_j)} + g_\xi(\boldsymbol{Z}_{jl},t) + \boldsymbol{Q}_{\xi jl}^{\boldsymbol{A}}, \tag{3.6}$$

$$\dot{g}_\xi(\boldsymbol{Z}_{jl},t) = \widehat{\boldsymbol{Q}}_{\xi jl}\Big(q\widetilde{\Phi}_{jl} - \frac{e}{c}\widetilde{\boldsymbol{V}_{jl}\cdot\boldsymbol{A}_{jl}}\Big). \tag{3.7}$$

This Kruskal ring is quickly changing with time in a plane perpendicular to the magnetic field and is different for each particle. Operator $\widehat{\boldsymbol{Q}}_\xi^{\boldsymbol{A}}$ is given by the following expression

$$\boldsymbol{Q}_\xi^{\boldsymbol{A}} \doteq \frac{q^2}{mc^2}\boldsymbol{A}\cdot\frac{\partial\boldsymbol{\rho}_0}{\partial\xi}. \tag{3.8}$$

The simulation is done self-consistently by calculating Maxwell's equations (2.11)-(2.12). The appropriate gyrophase integration in the current (2.13) is approximated by the summation over p ring-mates on each Kruskal ring. On the grid, the current takes the following form

$$\boldsymbol{J}_s(\boldsymbol{x},t) = \int d\boldsymbol{x}'\mathcal{S}(\boldsymbol{x}'-\boldsymbol{x})\boldsymbol{J}_s(\boldsymbol{x}',t), \tag{3.9}$$

where $\mathcal{S}(\boldsymbol{x}'-\boldsymbol{x})$ is the shape function (first-order particle weighting is used in this paper), and

$$\boldsymbol{J}_s(\boldsymbol{x}',t) = \sum_j\sum_{l=1}^{p}(\boldsymbol{v}_{\perp jl} + U_j\widehat{\boldsymbol{b}})[1 + g_{\mathsf{T}}(\boldsymbol{Z}_{jl},t) + \boldsymbol{Q}_{\mathsf{T}jl}^{\boldsymbol{A}}]\delta(\boldsymbol{X}_j - \boldsymbol{x}' + \boldsymbol{\rho}_{jl}). \tag{3.10}$$

The operator $\widehat{\boldsymbol{Q}}_{\mathsf{T}}^{\boldsymbol{A}}$ is defined by

$$\boldsymbol{Q}_{\mathsf{T}}^{\boldsymbol{A}} \doteq \frac{1}{m}\Big(\frac{\partial\ln F_0}{\partial\mu}\frac{\partial\boldsymbol{\rho}_0}{\partial\xi} + \frac{q}{mc}\frac{\partial\ln F_0}{\partial U}\widehat{\boldsymbol{b}}\Big)\cdot\boldsymbol{A} - \frac{\widehat{\boldsymbol{b}}}{B_0}\times\boldsymbol{A}\cdot\frac{\partial\ln F_0}{\partial\boldsymbol{X}}. \tag{3.11}$$

Since, numerically, the contributions to the current on the grid from the individual ring-mates are calculated separately, the $\boldsymbol{x}'$ integration and summation over ring-mates l in Eqs. (3.9)-(3.10) switch places. These operations commute since the shape function $\mathcal{S}(\boldsymbol{x}'-\boldsymbol{x})$ is gyrophase-independent.

The accuracy of this approximation is determined by the resolution of the gyrophase subspace by the total number of points p on each Kruskal ring. Particularly, for this approach, the number of points p we need to keep on each Kruskal ring for accurate estimation of averaged quantities is determined by the characteristic $k_\perp\rho$ we want to study in the system [15]. In conventional low frequency gyrokinetics, the evolution of the Kruskal rings is present implicitly in the polarization density term of the gyrokinetic Poisson equation [2].

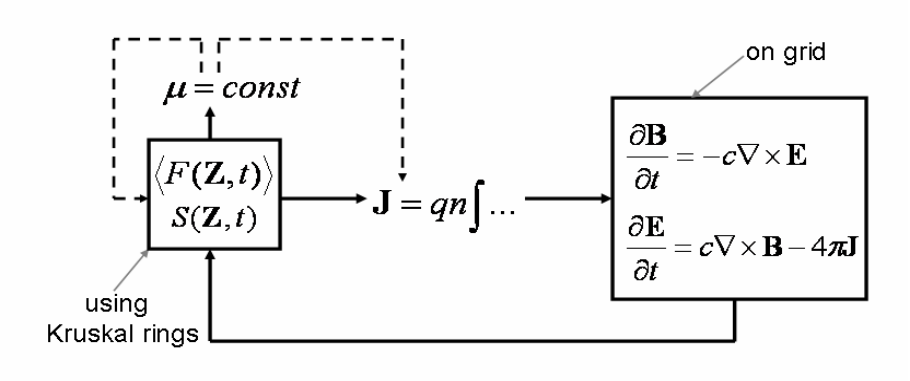

Figure 3: Schematic structure of the direct high frequency gyrokinetic algorithm.

Fig. 3 schematically shows how this direct high frequency gyrokinetic algorithm works. The gyrocenter and gyrophase dynamics is captured by $\langle F(\mathbf{Z},t)\rangle$ and $S(\mathbf{Z},t)$ functions through the evolution of the Kruskal rings. These quantities are used for calculation of the current $\boldsymbol{J}_s(\boldsymbol{x},t)$ from the Eq. (3.10). This current is then used in the Ampere's law, which is together with the Faraday's law is solved on the grid. The fields obtained from the Maxwell's equations are projected from the grid back to the Kruskal rings, thus closing the self-consistency loop. Conservation of the magnetic moment produces nonlinear effects in the form of the evolution of the Kruskal ring shapes.

To illustrate the new electromagnetic high frequency gyrokinetic algorithm, we shall use an example of the low-hybrid wave propagating in inhomogeneous magnetic field in 3D slab (Fig. 4). x is a direction of the magnetic field inhomogeneity. The ambient magnetic field is pointing in z direction, while its amplitude is decreasing as we move to the left in x direction away from the antenna. A simple antenna is located on the left surface to generate y (transverse) component of the electric field with the frequency $\omega = 200MHz$, which is above low-hybrid frequency near the antenna. As the wave propagates away from the antenna, it reaches the low-hybrid resonance. The size of the slab is $130cm \times 2\pi * 130cm \times 130/0.358cm$. The simulation is performed in a $200\times100\times8$-grid. Other parameters are the ion density $n_i = 0.17*10^{14} g/cm^3$, the magnetic induction $B_0 = 8.8*10^4 Gauss$.

As for the initial conditions, instead of loading a certain number of particles N_p as required by the Lorentz-force simulation, the high frequency gyrokinetic algorithm requires loading a certain number of gyrocenters N_{gc}. And for each of these gyrocenters, there must be a finite number of ring-mates p to approximate each Kruskal ring. The number of gyrocenters and the number of ring-mates can be chosen independently. The ion gyrocenters are distributed randomly in three spatial dimensions, while electrons ($s = e$) are treated according to the linear cold Ohm's law

$$\frac{\partial \boldsymbol{J}_s}{\partial t} = \frac{n_s q_s^2}{m_s}\boldsymbol{E} + \Omega_s \widehat{\boldsymbol{b}} \times \boldsymbol{J}_s \tag{3.12}$$

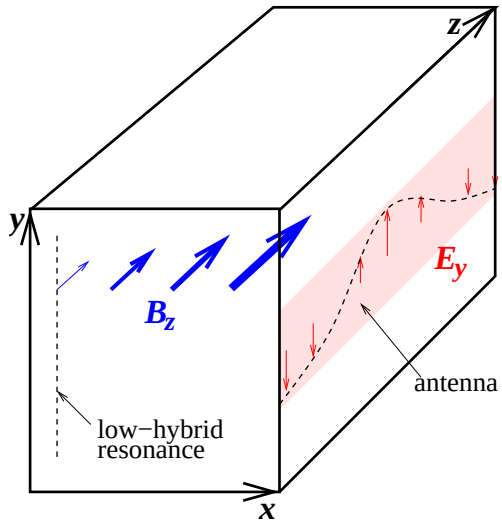

Figure 4: 3D slab used in simulation of the low-hybrid wave propagation. The wave is excited by the antenna and propagates in $-x$ direction toward low-hybrid resonance.

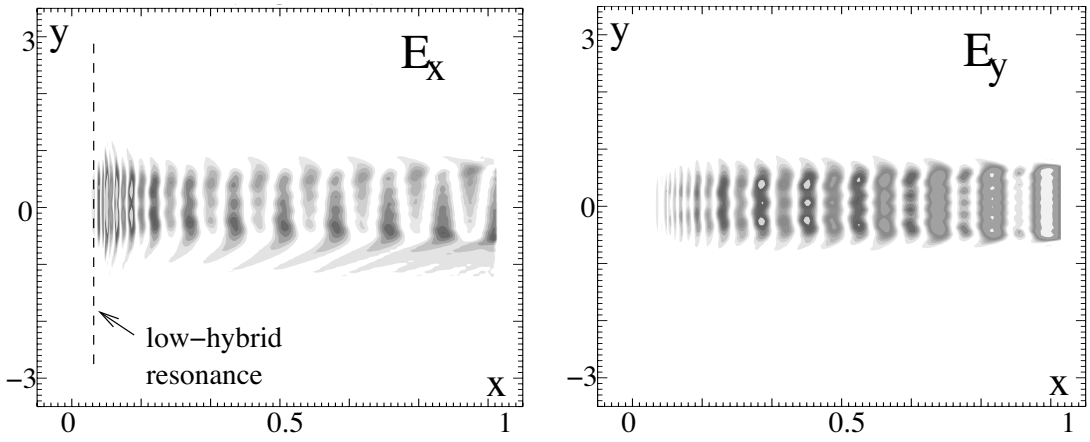

Figure 5: Longitudinal (E_x) and transverse (E_y) components of the electric field of the low-hybrid wave in (x,y) plane.

in both high frequency gyrokinetic and Lorentz-force simulations. Such cold approximation for the electrons is justified since finite electron FLR effects are not important for the dynamics of the low-hybrid wave we study in this paper.

Periodic boundary conditions were used in both y and z directions, while perfectly conducting boundary conditions were used for the x direction. Maxwell's equations together with the cold Ohm's law are solved on the grid using Yee's algorithm [19] together with locally implicit solver [20]. For this *field solver* part, the time step Δt must satisfy

$$\sqrt{(\Delta x)^2+(\Delta y)^2+(\Delta z)^2} > c\Delta t, \tag{3.13}$$

where Δx, Δy and Δz are grid cell sizes.

Fig. 5 in $x\times y$ cross-sections shows longitudinal and transverse components of the electric field of the low-hybrid wave. The ions are treated kinetically with the new algorithm and $N_{gc}=200$ gyrocenters were used with $p=4$ ring-mates for each Kruskal ring. The amplitude of the transverse component is decreasing as the wave approaches the resonance, where it becomes almost electrostatic.

The simple fact that the motion of gyrocenters is slow compared to the motion of ring-mates can make our new algorithm up to 6 times faster than a Lorentz-force simulation. Let us suppose that ΔT and Δt are the time steps used for solving gyrocenter and gyrophase equations respectively. The number of differential equations solved by the high frequency gyrokinetic code per each gyrophase time step is $(5\Delta t/\Delta T+p)N_{gc}$ (a gyrocenter and a ring-mate need five and one equations respectively), while the number of equations solved by the Lorentz-force code is $6N_p$. Using the constraint $N_p=pN_{gc}$ (resolution of the perpendicular dynamics is the same in both systems), we estimate that the former approach requires solving $6p/(5+p)$ times fewer differential equations. In the limits of slow gyrocenter motion ($\Delta t\ll\Delta T$),

$$\frac{pN_{gc}}{6N_p}\to\frac{1}{6}, \tag{3.14}$$

the gyrokinetic algorithm may be up to 6 times faster.

In the example in Fig. 5 we had $\Delta T=\Delta t$ with $\Delta t=6*10^{-12}s$ for the field solver as well as gyrocenter and gyrophase pushers. The total simulation time is $T=6*10^{-8}s$.

The only kinetic effect we will look at in this paper is the ion perpendicular stochastic heating. It is due to interaction between a wave and perpendicular particle motion. For the low-hybrid wave propagating in the x direction, this interaction mostly happens near the resonance, where the x component of the velocity is close to the wave phase velocity. From the high frequency gyrokinetic point of view, such interaction occurs whenever

$$v_x(\xi)=\omega/k_x \tag{3.15}$$

is satisfied between the ion Kruskal ring and the wave phase velocity (Fig. 6). If some decorrelation mechanisms are present, then particles will receive energy from the wave on average. To make sure we have this effect, we added an artificial decorrelation mechanism into the system. Particularly, each Kruskal ring gyrophase changes randomly occasionally.

In $x\times y$ plain, Fig. 7 shows the total perpendicular kinetic energy gained by ions in the end of the run due to stochastic heating in the low-hybrid wave (Fig. 5) with $N_{gc}=$ 200 gyrocenters and $p=4$ ring-mates. The stochastic heating is especially intensive near the resonance, since the phase velocity of the wave is decreasing as it approaches the resonance, and the majority of ions Kruskal rings can satisfy the resonant condition (3.15).

Direct high frequency gyrokinetic (or, alternatively, Lorentz-force) simulation requires a significant number of Kruskal-rings (particles) per cell for appropriate resolution of the

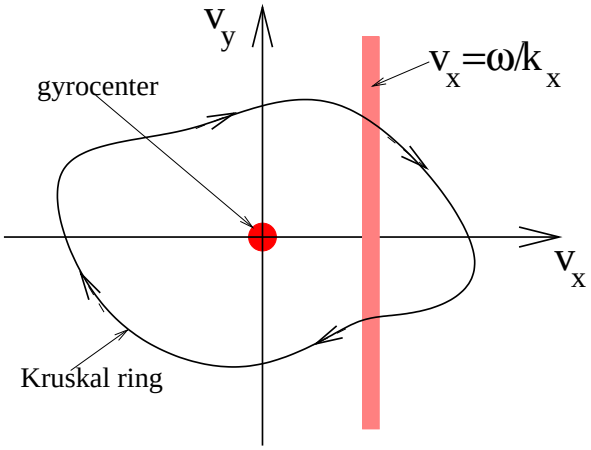

Figure 6: Mechanism of the ion perpendicular stochastic heating in the low-hybrid wave from the high frequency gyrokinetic point of view.

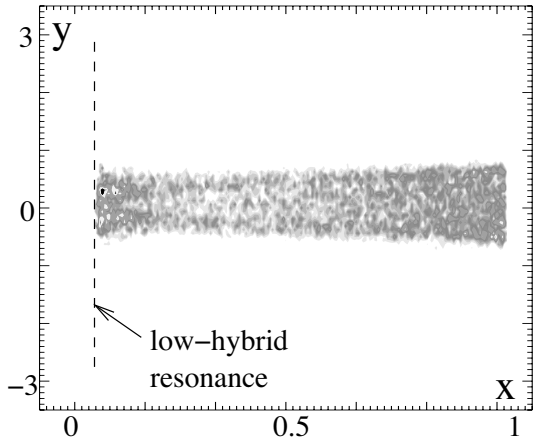

Figure 7: Total energy gained by ions due to perpendicular stochastic heating in the end of the run in (x,y) plane.

dynamics. Since the wave is excited locally (by the antenna), during its propagation it keeps the memory of its previous dynamics, and thus errors accumulate throughout the wave evolution.

The high frequency gyrokinetic formalism can offer us a way to avoid this by dividing the integral form of the current (2.13) into cold and kinetic contributions. Particularly,

$$\begin{aligned} \boldsymbol{J}_s(\boldsymbol{x},t) &= \int R_s(\boldsymbol{Z},t)\delta(\boldsymbol{X}-\boldsymbol{x}+\boldsymbol{\rho})d\boldsymbol{Z} \\ &= \int R_s(\boldsymbol{Z},t)\delta(\boldsymbol{X}-\boldsymbol{x})d\boldsymbol{Z}+\int R_s(\boldsymbol{Z},t)(\delta(\boldsymbol{X}-\boldsymbol{x}+\boldsymbol{\rho})-\delta(\boldsymbol{X}-\boldsymbol{x}))d\boldsymbol{Z}, \end{aligned} \tag{3.16}$$

where

$$R_s(\boldsymbol{Z},t)=q_s(\boldsymbol{v}_\perp+U\widehat{\boldsymbol{b}})[(1+\delta\mathrm{T})F_s(\boldsymbol{Z},t)]. \tag{3.17}$$

The first term on the right hand side of Eq. (3.16) produces cold response (zero perpendicular temperature)

$$\boldsymbol{J}_{cold}(\boldsymbol{x},t)=\int R_s(\boldsymbol{Z},t)\delta(\boldsymbol{X}-\boldsymbol{x})d\boldsymbol{Z} \tag{3.18}$$

when nonlinear terms are neglected. For this cold part instead of finding it directly from the Eq. (3.18) using particles, we might use linear cold Ohm's law (3.12). And only the kinetic part of the response

$$\Delta\boldsymbol{J}_{kinetic}(\boldsymbol{x},t)=\int R_s(\boldsymbol{Z},t)(\delta(\boldsymbol{X}-\boldsymbol{x}+\boldsymbol{\rho})-\delta(\boldsymbol{X}-\boldsymbol{x}))d\boldsymbol{Z} \tag{3.19}$$

needs to be solved using particles. If such separation is possible, the Kruskal rings in the system will be used only for the simulation of the deviation from the cold response instead of simulation all the dynamics how it is done in conventional Lorentz-force approach. This is similar to the δf-scheme, when some part of the dynamics like the background distribution function is either known or may be found analytically, and particle simulation only focuses on the deviation from this analytically known state. As a result, the total number of simulation particles may be dramatically reduced.

Fig. 8 schematically shows how such algorithm with divided cold and kinetic parts work. As before, the gyrocenter and gyrophase dynamics are determined by the Kruskal rings. The quantity $\Delta\boldsymbol{J}_{kinetic}(\boldsymbol{x},t)$ is then calculated, which is used in the Ampere's law. Maxwell's equations together with the cold Ohm's law for the ions are solved on the grid.

In Fig. 9, the light curve shows the same as Fig. 7 integrated over y direction, that is the total perpendicular energy gained by ions versus x in the end of the run from the direct simulation with $N_{gc}=200$ gyrocenters and $p=4$ ring-mates. The dark curve is from the simulation which utilized the separation between cold and kinetic effects in the current (3.16) with $N_{gc}=1$ gyrocenters and $p=4$ ring-mates. The dynamics of the stochastic heating is captured correctly by this approach. This method uses much smaller number of markers per cell and thus is much faster than the direct Lorentz-force like simulation. The gain is due to the fact that in the high frequency gyrokinetic simulation the Kruskal rings loaded in the system do not need to participate in resolution of the cold wave response.

4 Particle refinement

Another advantage our new high frequency gyrokinetic algorithm can give us is the possibility to have particle refinement together with mesh refinement in a system with different spatial scales. In our example of the low-hybrid wave propagating in the inhomogeneous magnetic field, we need higher grid resolution near the low-hybrid resonance, where the typical wave length becomes very short. This may be done by implementing

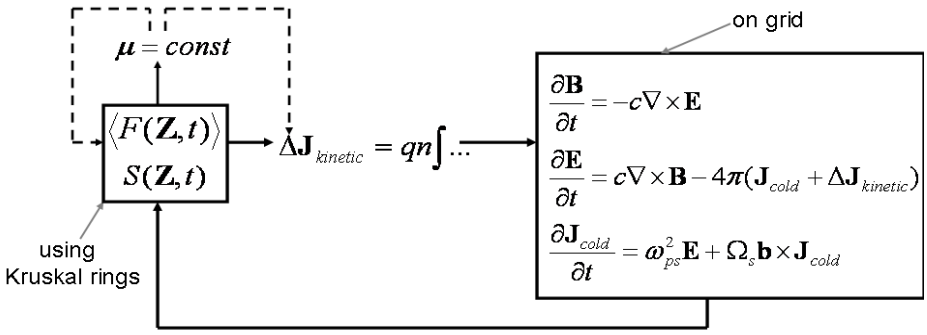

Figure 8: Schematic structure of the high frequency gyrokinetic algorithm with separated cold and kinetic parts in the current.

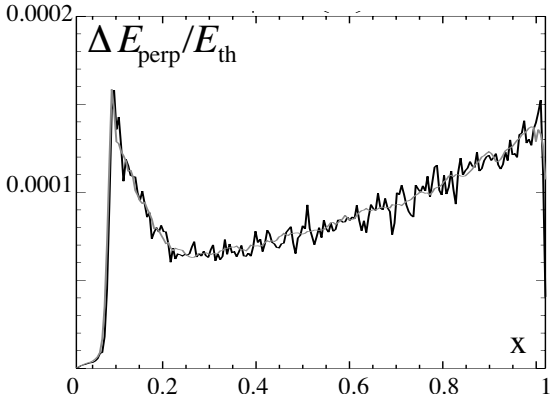

Figure 9: Total energy gained by the ions due to perpendicular stochastic heating in the end of the run versus x. The light curve is from the direct simulation, while the dark curve is from the simulation with separated cold and kinetic parts in the current.

some adaptive mesh refinement techniques [21], which makes sure to dynamically use finer grid when necessary.

Fig. 10 shows the regions where fine and coarse grid might be used. To imitate a mesh refinement technique, let us imagine that the cells in fine grid region are twice as smaller than the cells in coarse grid region, as shown in Fig. 10. This makes sure that we have twice as higher resolution in x direction in fine grid region. In a simulation where part of the dynamics is described by particles, the number of markers per cell must be approximately the same independent of the cell size. This is necessary to make sure that the resolution of the perpendicular velocity subspace is uniform in the system, independent of the grid structure. Particularly, the problems of wave propagation and convergence in fusion plasmas require an adequate treatment of FLR effects, and thus one must make sure that the short wavelength dynamics is resolved by sufficient number of particles. In a dynamically changing system, it would imply that we need to be able to dynamically add more markers locally in a region where the grid becomes finer and

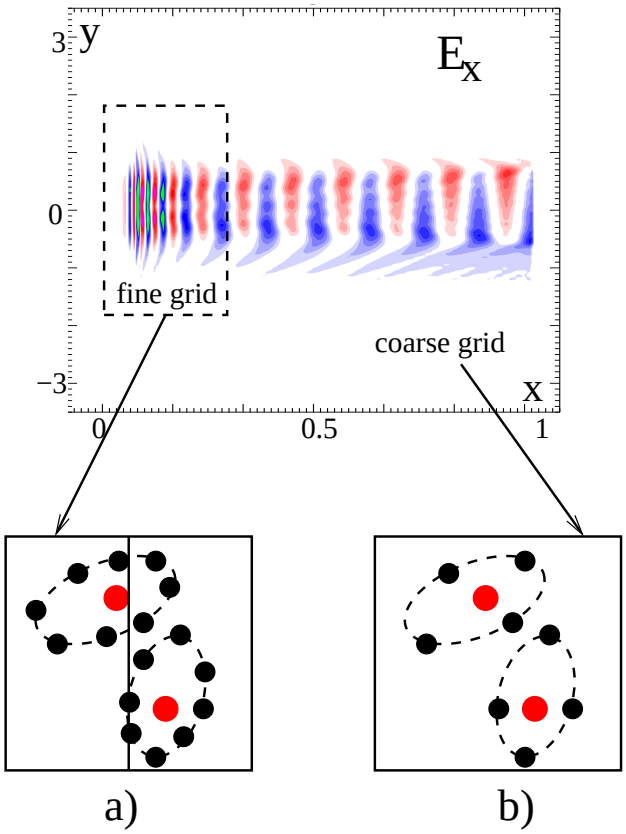

Figure 10: Dynamical particle refinement in the high frequency gyrokinetic algorithm. In the fine grid region (a) more ring-mates per gyrocenter are used than in the coarse grid region (b).

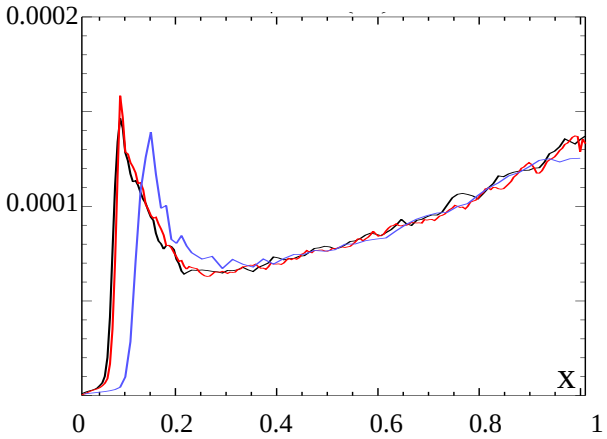

Figure 11: Total energy gained by the ions due to perpendicular stochastic heating in the end of the run versus x. The red curve is from the direct simulation with uniform fine grid. The blue curve is from the simulation with uniform coarse grid. The black curve is from the simulation which utilizes particle refinement technique together with mesh refinement technique.

remove extra markers in case if the grid becomes coarse again. Within Lorentz-force framework, such approach has been developed by Sydora *et al.* [21].

The new high frequency gyrokinetic algorithm offers a different way of doing perpendicular particle refinement. Particularly, let us imagine that in coarse grid region we have two Kruskal rings per cell, with each ring being approximated by four ring-mates (Fig. 10(b)). This is equivalent to having 8 markers per cell resolving perpendicular dynamics. Then in fine grid region with twice as smaller cells we need to have twice as higher marker density than in the surrounding coarse grid region (number of markers per cell must be the same everywhere in the system). There are two options. First, we can double the number of gyrocenters with the number of ring-mates fixed. Second, we can double the number of ring-mates for a fixed number of gyrocenters (Fig. 10(a)). The first option is similar to the Lorentz-force situation described above and involves generation of inhomogeneous gyrocenter density dynamically with the grid.

The second option is more suitable for our needs. Since we do not change the number of gyrocenters, they will stay uniformly distributed in the system regardless of what happens with the grid. At the same time, addition and removal of extra ring-mates is a straightforward task and can easily keep up with the grid to maintain the same number of markers per wavelength (same resolution of the perpendicular phase space) everywhere in the system. The drawback of this approach is that the resolution of the gyrocenter subspace decreases locally where the grid becomes finer. In hot plasmas it should not be a significant obstacle. This is due to the fact that the high frequency gyrophase dynamics is usually much noisier than the slow gyrocenter dynamics. As a consequence, many more markers are needed for the resolution of the perpendicular dynamics.

In Fig. 11, we treat our example of the ion stochastic heating using this method. The red curve was obtained, as before, from the well-resolved simulation, which used fine grid $\Delta x\times\Delta y\times\Delta z=130/200cm\times 2\pi*130/100cm\times 130/0.358/8cm$ everywhere in the system with 200 gyrocenters per cell (with 4 ring-mates).

The blue curve (Fig. 11) is from the simulation, which used coarse grid $2\Delta x\times\Delta y\times\Delta z$ everywhere in the system with the same number of gyrocenters and ring-mates. While this simulation is twice as fast (since the total number of particles in the system is twice as smaller), it does not capture the dynamics near the resonance correctly.

The black curve (Fig. 11) is from the simulation, which used fine grid $\Delta x\times\Delta y\times\Delta z$ near the resonance ($x\leq 0.3*130cm$), and coarse grid $2\Delta x\times\Delta y\times\Delta z$ away from the resonance ($x>0.3*130cm$). 100 gyrocenters (with 8 ring-mates) and 200 gyrocenters (with 4 ring-mates) per cell were used in fine and coarse grid regions, accordingly. By doing this, we make sure that both the gyrocenter density and the perpendicular resolution stay uniform in the system independent of the grid structure. This simulation captures the dynamics correctly and is 35% faster than the simulation which uses the fine grid (red curve).

Using realistic mesh refinement techniques together with particle refinement in our high frequency gyrokinetic algorithm can result in 10 times and more saving in computing time, compared to the Lorentz-force simulation with uniformly fine grid.

5 Discussion and future work

We developed an electromagnetic version of the high frequency gyrokinetic algorithm using gyrocenter-gauge kinetic theory, which allows one to simulate arbitrary frequency physics of strongly magnetized plasmas ($\rho/L_B \ll 1$). The algorithm solves the decoupled system of equations for the gyrocenter distribution $F(\boldsymbol{X},U,\mu,t)$ and gauge $S(\boldsymbol{Z},t)$ functions for $e\Phi/T \ll 1$. The high frequency gyrokinetics describes each particle as a combination of a gyrocenter and a complicated, quickly changing Kruskal ring. Similar to a direct Lorentz-force simulation, the new approach presented in this paper can self-consistently describe the wave dynamics together with the evolution of non-Maxwellian parts of distribution functions, particle orbits, etc. Also, it allows to address the issue of interaction between wave dynamics and microinstability-driven turbulence. In gyrokinetic formulation the perpendicular heating dynamics is completely described by the evolution of shapes of the Kruskal rings. The gyrokinetics naturally separates 1D gyrophase and 5D gyrocenter dynamics. This allows to use larger time steps to treat slower gyrocenter motion and thus saves computing time compared to the 6D Lorentz-force simulation. Also, separation of the cold response from the kinetic effects in the current allows one to reduce the total number of simulation particles. Possibility to have adaptive particle refinement together with mesh refinement allows to further reduce the number of particles in the systems with different spatial scales.

Acknowledgments

This work was supported by the Multi-Scale Gyrokinetics project as a part of the U. S. DoE ASCR Multiscale Mathematics Research and Education Program.

References

[1] R. G. Littlejohn, Phys. Fluids 24 (1981) 1730.
[2] W. W. Lee, Phys. Fluids 26 (1983) 556.
[3] T. S. Hahm, Phys. Fluids 31 (1988) 2670.
[4] R. A. Kolesnikov, W. W. Lee, H. Qin, E. Startsev, Phys. Plasmas 14 (2007) 072506.
[5] R. A. Kolesnikov, W. W. Lee, H. Qin, E. Startsev, 17th Topical Conference on Radio Frequency Power in Plasmas, American Institute of Physics, 2007, pp. 475-478.
[6] H. Qin, W. M. Tang, W. W. Lee, G. Rewoldt, Phys. Plasmas 6 (1999) 1575.
[7] H. Qin, W. M. Tang, W. W. Lee, Phys. Plasmas 7 (2000), 4433.
[8] H. Qin, C. K. Phillips, R. A. Kolesnikov, W. W. Lee et al., 17th Topical Conference on Radio Frequency Power in Plasmas, American Institute of Physics, 2007, pp. 471-474.
[9] X. S. Lee, J. R. Myra, P. J. Catto, Phys. Fluids 26 (1983) 223.
[10] G. Park, C. S. Chang, Phys. Plasmas 14 (2007) 152503.
[11] Z. Lin, T. S. Hahm, W. W. Lee, W. M. Tang, R. B. White, Science 281 (1998) 1835.
[12] E. F. Jaeger, L. A. Berry, J. R. Myra et al., Phys. Rev. Lett. 90 (2003) 195001.
[13] R. W. Harvey, O. Sauter, R. Prater, A. P. Nikkola et al., Phys. Rev. Lett. 88 (2002) 205001.

[14] M. Choi, V. S. Chan, R. I. Pinsker, S. C. Chiu, W. W. Heidbrink, Phys. Plasmas 12 (2005) 2505.
[15] W. W. Lee, J. Comput. Phys. 72 (1987) 243.
[16] S. E. Parker, W. W. Lee, Phys. Fluids B 5 (1993) 77.
[17] H. Qin, Fields Institute Communications 46 (2005) 171.
[18] M. Kruskal, J. Math. Phys. 3 (1962) 806.
[19] K. S. Yee, IEEE Transactions on antennas and propagation AP-14 (1966) 302.
[20] D. N. Smithe, A. H. Hakim, 17th Topical Conference on Radio Frequency Power in Plasmas, American Institute of Physics, 2007, pp. 483-486.
[21] R. Sydora, 20th International Conference on Numerical Simulation of Plasma, 2007, in press.